Probabilistic Engineering Mechanics 54 (2018) 9–24

Contents lists available at ScienceDirect

Probabilistic Engineering Mechanics

journal homepage: www.elsevier.com/locate/probengmech

A refined analysis of thunderstorm outflow characteristics relevant to the wind loading of structures

Shi Zhang [a], Giovanni Solari [b,*], Patrizia De Gaetano [b], Massimiliano Burlando [b], Maria Pia Repetto [b]

[a] Beijing's Key Laboratory of Structural Wind Engineering and Urban Wind Environment, School of Civil Engineering, Beijing Jiaotong University, Beijing 100044, China
[b] Department of Civil, Chemical and Environmental Engineering (DICCA), Polytechnic School, University of Genoa, Via Montallegro, 1, 16145 Genoa, Italy

ARTICLE INFO

Keywords:
Monitoring network
Signal analysis
Synoptic event
Thunderstorm outflow
Wind dataset
Wind loading

ABSTRACT

The study of thunderstorm outflows and their loading and response of structures is a key topic in modern wind engineering. This paper provides a new contribution to this research by analyzing a wide dataset of 277 wind velocity records characterized by strong transient properties and labeled by thunderstorm outflow. These records have been detected for up to 6 years by 14 anemometers belonging to an extensive in-site monitoring network distributed in the Northern Mediterranean ports. Analyses are carried out in order to extract the parameters of major interest for evaluating the wind loading effects of structures and furnishing a comprehensive statistical characterization of the huge amount of data recorded. Results lead to a novel classification of thunderstorm outflows with reference to the time scale of the gust front passage and their intensity; a refined interpretation of the differences involved by the turbulence intensity, the integral length scale and the gust factor of mesoscale downbursts and synoptic low-pressure systems; a confirmation of the substantial independence of these quantities with respect to the ratio between the height above ground of the sensor and the roughness length of the terrain, together with their correlation with the wind velocity; a new parameterization of the harmonic content of the turbulent fluctuations.

1. Introduction

The study of thunderstorm outflows and their loading of structures is a key topic of modern wind engineering [1,2]. This depends mainly on the fact that the methods currently used to determine the wind actions on structures are still mostly based on the synoptic extra-tropical cyclone model introduced by Davenport in 1961 [3]; this model assumes neutral atmospheric conditions, statistical stationarity features and wind velocity profiles in equilibrium with the atmospheric boundary layer (ABL). Thunderstorm outflows are transient phenomena at the mesoscale [4,5] that occur in convective conditions with "nose" velocity profiles [6] totally different from those that are typical of the ABL. Several studies show that the design wind velocity is often linked with thunderstorm events [7–11].

The literature is rich in contributions that illustrate measurements of thunderstorm outflows whose analysis is carried out in order to extract their parameters of major interest for evaluating the wind loading of structures. Refs. [12–14] describe the results of a monitoring program in Singapore, which gave particular remark to the definition and values of the gust factor. Ref. [15] analyzes the time evolution of the vertical profile of the mean wind velocity and the turbulence properties of transient events registered in the north-European coastal areas. Ref. [16] investigates the space–time properties of the rear-flank downdraft of a super-cell and of a derecho detected in a thunderstorm outflow experiment conducted in 2002 in Lubbock, Texas. Inspecting the same rear-flank downdraft, Ref. [17] develops the decomposition of its velocity in a moving average mean and a residual turbulent component whose characteristics are examined in detail. Similar evaluations are reported in [18] with reference to a downburst occurred in 2004 at the SMEAR II Station in Finland. Ref. [19] investigates some thunderstorms that occurred in Lubbock in order to elucidate their properties relevant to wind engineering. Ref. [20] depicts high-resolution field measurements of thunderstorm outflows carried out at Texas Tech University by means of surface instruments and mobile Doppler radars.

Despite these and many other analyses, the understanding, the representation and the modeling of thunderstorm outflows are still full of uncertainties and problems to be clarified. On the one hand, the

* Corresponding author.
E-mail address: giovanni.solari@unige.it (G. Solari).

http://dx.doi.org/10.1016/j.probengmech.2017.06.003
Received 15 June 2017; Accepted 21 June 2017
Available online 8 July 2017
0266-8920/

complexity of these atmospheric phenomena makes very difficult to formulate models that are physically realistic and simply applicable as in the case of synoptic depressions. On the other hand, their short duration and small size make very limited the available data, precluding the possibility of carrying out, as in the case of synoptic events, robust statistical evaluations and interpretations of the signals detected [21,22].

The projects "Wind and Ports" (WP) [23] and "Wind, Ports and Sea" (WPS) [24] represent a unique opportunity to contribute to the growth and the advance in the knowledge of thunderstorm outflows and their parameters relevant to the wind loading of structures. Started in 2009 and finished in 2015, these projects were financed by the European Territorial Cooperation Objective, Cross-border program "Italy-France Maritime 2007–2013". They involved the Port Authorities of the five main commercial ports in the Northern Tyrrhenian area, namely Genoa, La Spezia, Livorno, Savona– Vado Ligure (Italy) and Bastia–L'Île Rousse (France). The Department of Civil, Chemical and Environmental Engineering (DICCA) of the University of Genoa was the only scientific partner. These projects focused on the wind forecast and developed an integrated system made up of an extensive in-site monitoring network, an unprecedented dataset of wind measurements, the numerical simulation of wind and wave fields, the statistical analysis of the wind climate, an algorithm for the medium term (1–3 days) wind and wave forecast, and an algorithm for the short-term (0.5–2 h) wind forecast. Results are available to port operators by an integrated web-based GIS system for the safe management of port areas. The prosecution of this activity after 2015 is regulated by a Memorandum of Understanding between the University of Genoa and the Port Authorities involved in the above projects.

Thanks to the WP and WPS wind monitoring network and working on the wind dataset that it generated, a semi-automatic procedure was implemented to recognize and extract thunderstorm outflow records [25]. By means of this procedure a preliminary set of 93 records, labeled as thunderstorm outflows, was gathered from measurements carried out for 2 years by 9 anemometers. These records were decomposed into the sum of a slowly-varying mean wind velocity plus a residual fluctuation. In turn, the fluctuation was expressed as the product of its slowly-varying standard deviation by a reduced turbulent fluctuation dealt with as a rapidly-varying random stationary process with zero mean value and unit standard deviation. The extraction of the mean value and of the standard deviation were carried out by a moving average filter with period 30 s. Special attention was dedicated to the duration of the gust front passage, turbulence intensity, power spectral density, integral length scale and gust factor [26]; all these analyses were carried out comparing the statistical parameters of the selected thunderstorm outflows with those of 229 synoptic wind records. These properties formed the base to formulate two novel methods for determining the structural response to thunderstorm outflows: the first represents a generalization of the response spectrum technique widely used in the seismic field [27,28]; the second involves time-domain integrations based upon a so-called hybrid simulation technique of the thunderstorm outflow wind field [29].

In the meanwhile, the monitoring network has been enhanced with other instruments and new analyses have been performed on the records gradually acquired. This led to gathering a broader and more controlled dataset, including 277 records of thunderstorm outflows and other events with highly transient properties as extracted from measurements carried out for up to 6 years by 14 anemometers. This paper describes the analyses of this data repeating, improving, extending and often changing the methods applied in the previous study [26] on the basis of the new experience and knowledge acquired.

In particular, Section 2 illustrates the main properties of the wind monitoring network and of the measured wind dataset. Section 3 describes the criterion by means of which intense wind events are separated and thunderstorm outflows are extracted and cataloged. Section 4 depicts the method used to decompose thunderstorm outflow signals into component parts whose statistical properties are later on evaluated. Accordingly, Sections 5–7 examine the slowly-varying mean wind velocity, the turbulence intensity and the reduced turbulent fluctuations, respectively. Sections 8 and 9 discuss the turbulence intensity modulation and some noteworthy wind velocity ratios. Section 10 summarizes the main conclusions and provides some prospects for future research.

2. Monitoring network and wind dataset

Fig. 1 shows an outline of the in-site wind monitoring network created by the WP [23] and WPS [24] European Projects. The yellow circles correspond to the first 23 ultrasonic bi- or tri-axial anemometers, distributed in the Ports of Genoa (2), La Spezia (5), Livorno (5), Savona–Vado Ligure (6) and Bastia (5) in the course of the WP Project. The orange circles refer to 5 new ultra-sonic anemometers mounted in the Ports of Savona (1), La Spezia (1), Livorno (1) and L'Île Rousse (2) during the WPS Project. Still in the frame of the WPS Project, the monitoring network has been enlarged by adding 3 weather stations (blue circles), each one including another ultra-sonic anemometer, one barometer, one thermometer and one hygrometer, and 3 LiDAR (Light Detection And Ranging) (red circles), which detect the wind velocity profile from 40 to 250 m above ground level (AGL). Other sensors autonomously installed by single Port Authorities are in the stage of becoming integral parts of the WP and WPS network.

The instruments are distributed in order to homogeneously cover the port areas involved in these projects. To avoid local effects and to register undisturbed wind velocities, they are mounted at least at 10 m height AGL, mainly on high-rise towers or, in few cases, on antenna masts at the top of buildings. Wind measurements are recorded with a precision of 0.01 m/s and 1° for the intensity and direction, respectively. The sampling rate is 10 Hz with the exception of the anemometers in the port area of Bastia–L'Île Rousse, whose sampling rate is 2 Hz. Table 1 shows the main properties of the 31 ultra-sonic anemometers at present available; h is the height of the sensors AGL. A description of the LiDAR properties is given in [24].

A set of local servers placed in each Port Authority headquarter receives the data acquired by the anemometers in their own port area and elaborates their basic statistics on 10-min periods, namely the mean and peak wind velocities and the mean wind direction. Each server automatically sends this information to the central server at DICCA that carries out a preliminary check of the quality of the data, then stores it into a central dataset.

Table 1 shows periods of measurements varying from anemometer to anemometer. This depends, first of all, on the successive installation of the instruments. In addition, there are several periods in which measurements have been not carried out due to accidents or malfunctions of the instruments, these including some cases in which sensors have not been restored yet. Of course, there are also periods in which measurements have been not enough reliable to be examined [30,31]. Finally, taking into account the burden of the analyses described in this paper, the data provided by several sensors has not been studied yet; more precisely, at present analyses have been carried out for 14 sensors out of 31 available. The last column of Table 1 provides the percentage of the examined data for each examined instrument. Obviously, the correctness and reliability of the dataset is fundamental to carry out correct and reliable signal analyses.

Some preliminary evaluations on the data detected by the LiDAR profilers are illustrated in [32].

3. Extraction and classification of thunderstorm outflows

Coherently with modern trends in mixed wind climate conditions [2,11,33,34], the separation and classification of intense wind events into homogeneous categories is a fundamental preliminary step to carry out refined analyses of different phenomena and of their loading and response of structures. In principle, this separation calls for the joint

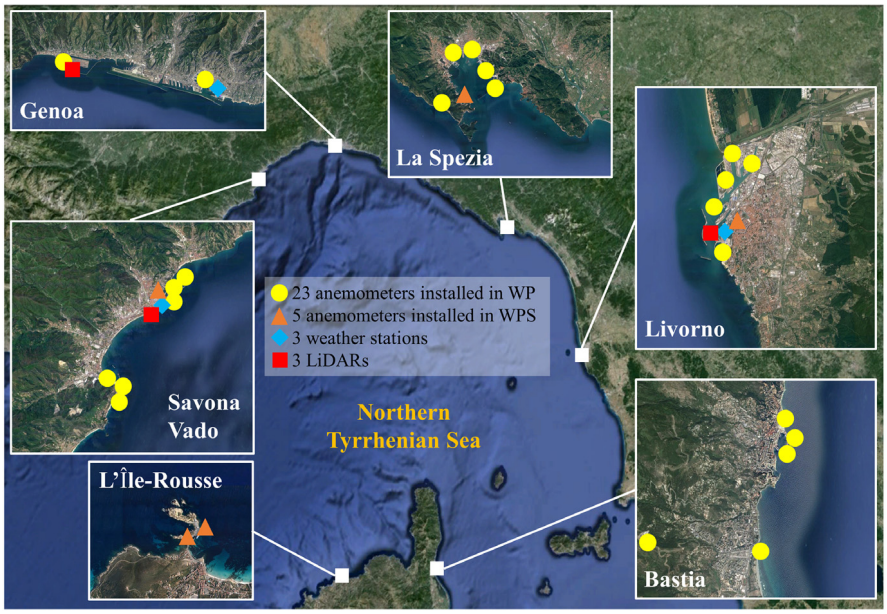

Fig. 1. WP and WPS wind monitoring network.

Table 1
Main properties of the ultrasonic anemometers of the monitoring network.

Port	Anem. No.	*h* (m)	Type	Period of measurement	Period of analysis	Valid data (%)
Savona–Vado	0	84	tri-axial	2011.03.30–now	–	
	1	33.2			2014.12.01–2016.01.31	87%
	2	12.5			2014.12.01–2016.01.31	72%
	3	28			2014.12.01–2016.01.31	83%
	4	32.7			2014.12.01–2016.01.31	86%
	5	44.6			2014.12.01–2016.01.31	87%
	6	10	bi-axial	2014.04.05–now	–	
	7	35		2015.07.31–now		
Genoa	1	61.4	bi-axial	2011.03.30–2013.05.07	2011.03.30–2013.04.01	59%
	2	13.3		2010.10.12–2015.05.31	2010.10.12–2015.05.31	56%
	3	32		2015.04.16–now	-	
La Spezia	1	15.5	bi-axial	2010.10.29–now	-	
	2	13			2010.10.29–2015.12.31	88%
	3	10		2011.02.04–now	2011.02.05–2015.12.18	89%
	4	11		2011.04.14–now		
	5	10		2012.09.06–now	–	
	6	16		2015.01.23–now		
Livorno	1	20	tri-axial	2010.09.16–now	2010.10.01–2015.12.12	86%
	2	20			2010.10.01–2015.12.12	67%
	3	20		2010.09.16–2015.03.21	2010.10.01–2015.03.21	74%
	4	20		2010.09.16–now	2010.10.01–2015.12.12	60%
	5	75		2010.09.16–2014.08.25	2010.10.01–2014.08.25	69%
	6	12	bi-axial	2015.07.25–now	–	
	7	23.8				
Bastia	1	10	bi-axial	2011.11.17–now	–	
	2	10				
	3	13				
	4	10				
	5	10				
L'Île-Rousse	1	10	bi-axial	2015.06.03–now	–	
	2	10		2015.06.08–now		

study of the records detected by a wind monitoring network and the weather scenarios in which such events take place; in the reality this approach is as powerful as burdensome and looks forward to future developments currently in the embryonic stage [35]. Accordingly, the process of wind velocity records by means of synthetic indicators and expert judgments is still the only reasonable pathway to separate and classify an extensive amount of data [8–11,13,15,34,36].

In order to achieve this goal as efficiently as possible, a semi-automated procedure was developed in [25] that establishes a censoring velocity threshold and separates the dataset of the anemometric records whose peak wind velocity exceeds that threshold into three selective sub-datasets referred to as stationary Gaussian extra-tropical cyclones, non-stationary non-Gaussian thunderstorm outflows, and stationary non-Gaussian intermediate events. This procedure was applied in [26] to the 10-min records detected by 9 ultra-sonic anemometers in the period 2011–2012, whose 1-s peak was greater than 15 m/s. In that study, the use of synthetic parameters was mainly circumscribed to the gust factors; the expert judgment involved the visual check of both

Table 2
Number of thunderstorm events (NTE) and records (NTR) examined.

Port	Anem. No.	NTE	NTR	10 min	1 h	10 h
Genoa	1	41	9	5	4	0
	2		34	11	18	5
Livorno	1		40	19	14	7
	2		20	8	9	3
	3	84	28	15	9	4
	4		39	18	19	2
	5		16	6	8	2
Savona and Vado	1		5	3	2	0
	2		3	1	2	0
	3	23	7	6	0	1
	4		10	7	2	1
	5		4	2	1	1
La Spezia	2	50	20	12	8	0
	3		42	28	10	4
Total	14	198	277	141	106	30
Percent	–	–	100%	50.9%	38.3%	10.8%

10-min and 1-h records centered around the peak wind speed. The use of a relatively low censoring threshold is coherent with the wind engineering tradition of investigating the properties of intense synoptic wind events by collecting all records that satisfy the requirement of neutral atmospheric conditions [21,22]. In [26] 93 transient velocity records related to convective conditions and thunderstorm outflows were extracted; this made possible to carry out preliminary statistical evaluations of their parameters.

The above procedure is herein extended to the data recorded by 14 ultra-sonic anemometers (Table 2) (including the 9 previously studied) in the period 2010–2016. In addition, following the method proposed in [37], analyses have been improved by selecting thunderstorm outflows based not only on 10-min and 1-h records, but also on 10-h records centered on the considered 10-min record. On the whole this approach led to extract 277 strongly non-stationary records (NTR) that, likewise and better than the previous ones, can be traced back to convective conditions and thunderstorm outflows, this involving not only the assemblage of a more controlled thunderstorm sub-dataset but also a major advance in understanding the thunderstorm time-scale, duration and type. Obviously, there are more NTR than thunderstorm events (NTE) since the same thunderstorm event may be detected by two or more anemometers in the same port area [35] due to the size and translational velocity of the thunderstorm cells. Research is in progress to extend this procedure to LiDAR measurements [32].

The loading and response of structures to transient convective gust fronts depends on three main parameters [38]: (1) the peak wind velocity; (2) the duration of the non-stationary part of the wind velocity and its ramp-up; and, (3) the shape of the wind velocity profile.

Accordingly, thunderstorm outflows are first separated into three families depending on whether the presence of a ramp-up and a transient peak are clearly detectable over a 10-min, 1-h or 10-h long records; for sake of simplicity they are referred to as “10-min”, “1-h” and “10-h” thunderstorms. Figs. 2–4 show three typical events belonging to these three families, respectively. For each event the pictures (a), (b) and (c) show, respectively, the time-history of the wind speed in a 10-min, 1-h and 10-h time period indicatively centered around the gust peak. In particular, picture (a) illustrates the mean velocity v_{m10} over a 10-min period (horizontal line) and the peak velocity $\hat{v}$ averaged on $\tau = 1$ s (circle) (obviously smaller than the instantaneous peak); picture (b) shows the mean velocity v_{m60} over a 1-h period (horizontal line), the variation of the mean velocity over 10-min subsequent periods (dotted line), and the 1-s peak (circle); picture (c) shows the evolution of the mean velocity over 10-min subsequent periods (dotted line).

In addition, thunderstorm outflow records have been separated into 4 groups as a function of the 1-s peak wind speed value. Table 3 shows the results of this classification pointing out, at least for the available data, no clear systematic correlation between the duration of the gust front passage and the peak wind speed. It is worth noting, however, that the peak wind speed of 1/3 of all the NTRs is greater than 20 m/s and the 4 events whose peak wind speed exceeds 30 m/s have a short duration. Authors hope that the acquisition of new measurements by LiDAR [32] makes possible, in a near future, to study the correlation between the shape of the vertical profile of the wind speed, its peak value and the ramp-up duration.

In the following sections the study of the statistical properties of the detected wind velocity signals is restricted to 247 10-min and 1-h thunderstorms, thus excluding 30 10-h thunderstorms (Table 2). Meteorological studies currently in progress point out that at least a relevant part of these events cannot be defined as thunderstorms and, in any case, their duration is so long as to prevent significant transient effects on structures.

4. Decomposition of wind velocity signals

For the sake of analyzing the statistical properties of thunderstorm outflow records, the horizontal component of the wind speed is expressed here by the classical decomposition rule [17,26,38–41]:

$$v(t) = \bar{v}(t) + v'(t) \tag{1}$$

where $t \in [0, \Delta T]$ is the time being $\Delta T = 10$ min, $\bar{v}$ is the slowly-varying mean wind velocity whereas v' is the residual turbulent fluctuation:

$$v'(t) = \sigma_v(t)\,\tilde{v}'(t) \tag{2}$$

where σ_v is the slowly-varying standard deviation of v' and $\tilde{v}'$ is the reduced turbulent fluctuation. Here and in the following an over-bar denotes a temporal average over ΔT.

Several methods are currently available in order to extract $\bar{v}$ from v [41,42]. Likewise in [26] this operation is here carried out by a rather classic moving average filter or running-mean [17,39] with a moving average period $T = 30$ s. The same criterion is used to extract σ_v from v'.

Replacing Eq. (2) into Eq. (1), the wind velocity v results:

$$v(t) = \bar{v}(t)\left[1 + I_v(t)\,\tilde{v}'(t)\right] \tag{3}$$

where:

$$I_v(t) = \frac{\sigma_v(t)}{\bar{v}(t)} \tag{4}$$

is the slowly-varying turbulence intensity.

Let us express the slowly-varying mean wind velocity and turbulence intensity as:

$$\bar{v}(t) = \bar{v}_{\max}\,\gamma(t) \tag{5}$$

$$I_v(t) = \bar{I}_v\,\mu(t) \tag{6}$$

where $\bar{v}_{\max}$ is the maximum value of $\bar{v}$ whereas γ is a non-dimensional function of t that defines the slow time variation of $\bar{v}$, being $\gamma_{\max} = 1$; $\bar{I}_v$ is the average value of I_v in ΔT whereas μ is a non-dimensional function of t that defines the slow time variation of I_v, being $\bar{\mu} = 1$.

Replacing Eqs. (5) and (6) into Eq. (3) the signal decomposition may be re-written as:

$$v(t) = \bar{v}_{\max}\gamma(t)\left[1 + \bar{I}_v\mu(t)\,\tilde{v}'(t)\right]. \tag{7}$$

Table 4 shows the mean and standard deviation values of $\mu_{v'}$ scaled by the peak value $\hat{v}'$ of v'. These values are separated into three families that comprehend the 10-min and 1-h thunderstorms as well as both. It is apparent that both the mean and the standard deviation values of $\mu_{v'}/\hat{v}'$ are nearly zero; this confirms that assuming a moving average period $T = 30$ s is an appropriate and rational choice. It is also worth noting

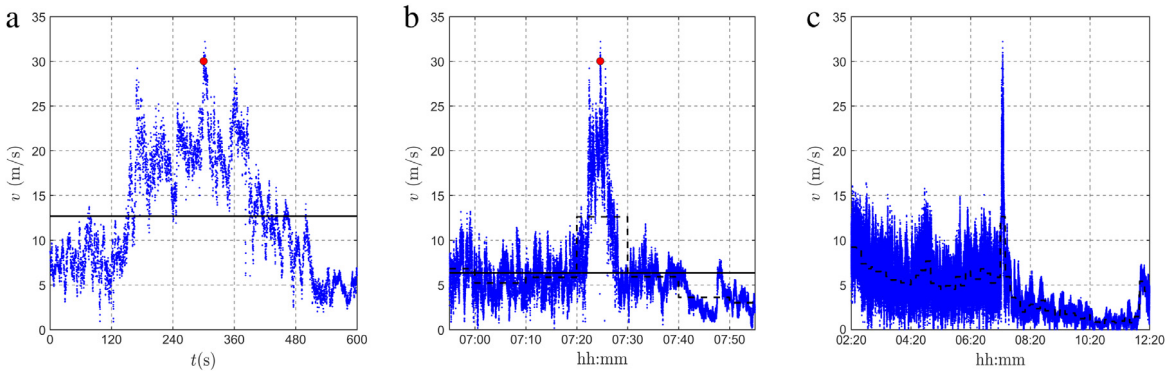

Fig. 2. "10-min" thunderstorm outflow record (Anemometer 2, Port of La Spezia, 07:20, 11 April 2012): velocity in a 10-min period (a), in a 1-h period (b) and in a 10-h period (c).

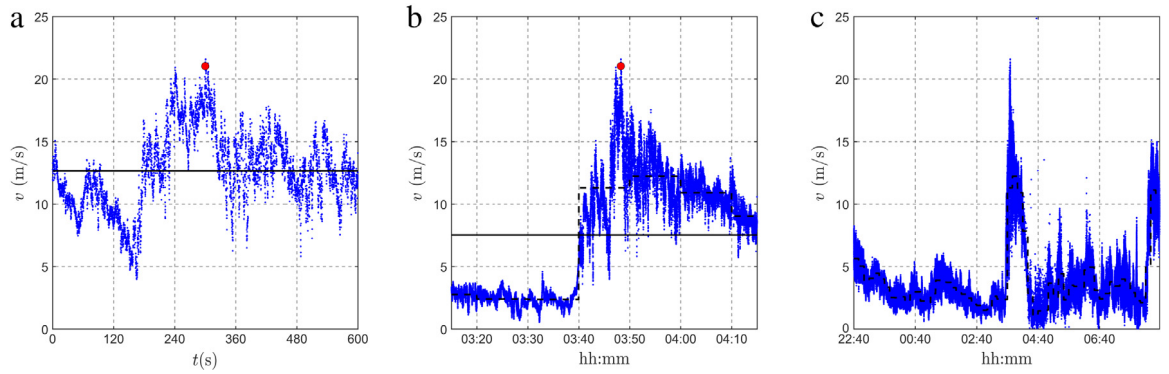

Fig. 3. "1-h" thunderstorm outflow record (Anemometer 1, Port of Livorno, 03:40, 21 July 2014): velocity in a 10-min period (a), in a 1-h period (b) and in a 10-h period (c).

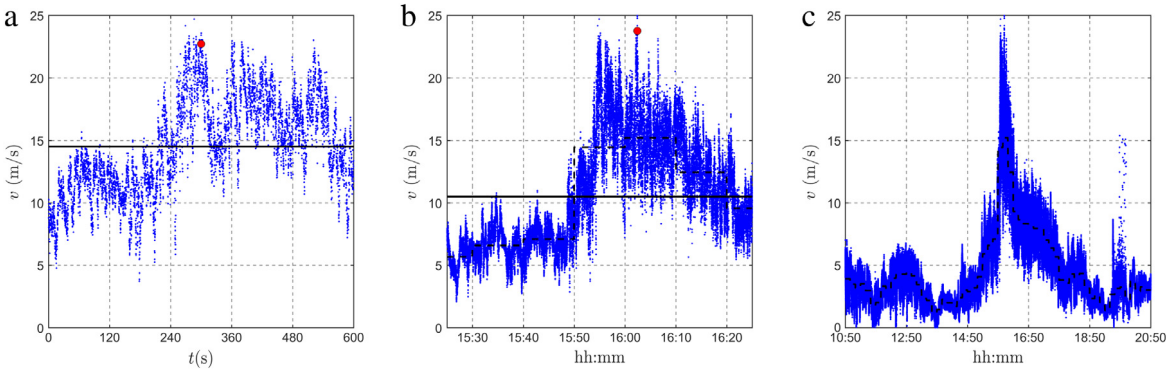

Fig. 4. "10-h" thunderstorm outflow record (Anemometer 2, Port of Livorno, 15:50, 4 September 2011): velocity in a 10-min period (a), in a 1-h period (b) and in a 10-h period (c).

that the above three families of thunderstorm records involve similar values. Here and in the following $\langle\bullet\rangle$, $\mathrm{std}(\bullet)$, $\mathrm{cov}(\bullet)$ denote the mean, the standard deviation and the coefficient of variation (if applicable), respectively, over an ensemble of thunderstorm records.

Fig. 5 elucidates the harmonic content of the component parts in which the original thunderstorm signals have been decomposed. Each picture shows the diagram of the function $n\left\langle\left|F_\xi(n)\right|^2\right\rangle$, where n is the frequency and $F_\xi(n)$ is the Fourier transform of $\xi(t)$, being $\xi = v, \bar{v}, v', \sigma_v, I_v, \widetilde{v}', \gamma, \mu$ (Fig. 5(a)–(h)); black and gray lines refer to 10-min and 1-h thunderstorms, respectively. As expected, $\xi = v, \bar{v}, \sigma_v, I_v, \gamma, \mu$ have a low frequency harmonic content whereas $\xi = v', \widetilde{v}'$ (Fig. 5(c), (f)) have a high frequency harmonic content. It is also worth noting that the harmonic content of the component parts of the 1-h thunderstorms tends to be slightly shifted towards the right of the 10-min ones; the differences, however, are very small.

5. Slowly-varying mean wind velocity

The records labeled here as thunderstorm outflows are characterized by a prominent peak whose duration has a dominant role in the wind loading and response of structures [38]; it corresponds to the gust front passage and it is best described by the slowly varying mean wind velocity $\bar{v}(t)$ or, more precisely, by the non-dimensional function $\gamma(t)$ (Eq. (5)) [26].

Fig. 6 shows the ensemble of the diagrams of γ for all the 10-min (a) and 1-h (b) thunderstorm records investigated; the thick lines refer to the mean value of γ as a function of time. This figure confirms what was already noted in [26]: due to the great variability of the functions γ, they can be regarded as samples of a non-stationary random process. The mean values of γ in the pictures (a) and (b) sum up the essential features of a sudden ramp-up and down in the wind speed; they are very similar in proximity of the peak whereas their difference is apparent

Table 3
Classes of membership of the peak wind velocity of thunderstorms.

Duration	Port	15–20 (m/s)	20–25 (m/s)	25–30 (m/s)	30–35 (m/s)	Total
10 min	GE	11	3	2	0	16
	LI	42	20	2	2	66
	SV	12	6	1	0	19
	SP	23	11	4	2	40
	Total	**88 (63%)**	**40 (28%)**	**9 (6%)**	**4 (3%)**	**141**
1 h	GE	19	3	0	0	22
	LI	40	16	3	0	59
	SV	5	0	2	0	7
	SP	14	3	1	0	18
	Total	**78 (73%)**	**22 (21%)**	**6 (6%)**	**0 (–)**	**106**
10 h	GE	4	1	0	0	5
	LI	10	6	2	0	18
	SV	3	0	0	0	3
	SP	3	1	0	0	4
	Total	**20 (67%)**	**8(27%)**	**2 (7%)**	**0 (–)**	**30**
NTR		186	70	17	4	277

Table 4
Mean and std values of $\mu_{\dot{v}'}/\hat{v}'$ for different families of thunderstorms.

Family	10 min	1 h	Both
Mean($\mu_{\dot{v}'}/\hat{v}'$)	0.0000	0.0003	0.0002
Std($\mu_{\dot{v}'}/\hat{v}'$)	0.0018	0.0018	0.0018

far from it. In particular, the definition of the peak duration provided in [26], namely the period in which γ is greater than or equal to 0.6, confirms that 1-h thunderstorms last clearly more than the 10-min ones. In both cases the inner envelopes of the γ diagram closely approximate the half-sine wave function introduced in [38] in order to model $\bar{v}(t)$.

The number of thunderstorm signals detected with high sampling rate offers authors the opportunity to establish a preliminary description of the most recurrent shapes of the slowly-varying mean wind velocity time histories.

The family of the 10-min thunderstorm records presents a large variety of shapes, whose features could in principle affect the structural response. Fig. 7 depicts some examples of the dominant shapes, showing the 20-min time histories of the wind speed centered around the 1-s peak. The most frequent shape is similar to a single spike lasting 2 to 3–4 min approximately, as shown in Fig. 7(a), (b). Note that the highest slope of the spike can occur during the ramp-up (Fig. 7(a)) as well as during the drop-off, after the maximum (Fig. 7(b)). A second recurrent shape presents a plateau after a very steep ramp-up that lasts about 4–5 min, as shown in Fig. 7(c), (d). Instead of a single maximum, the plateau is characterized by many secondary peaks. Fig. 7(e), (f) shows less frequent shapes, characterized by two well distinguished peaks (Fig. 7(e)) or by relatively mild increasing/decreasing ramps (Fig. 7(f)). A common feature of all these 10-min signals is that they have a lower background wind speed before and after the stronger event's occurrence, which represents the mean background flow that these short-living thunderstorms are embedded into.

The family of the 1-h thunderstorm records may be drawn back to some recurrent shapes depicted through the examples in Fig. 8, which shows the 2-h time histories of the wind speed centered around the 1-s peak. The first group is characterized by a strong event lasting approximately 20–40 min as shown in Fig. 8(a), (b); also in these cases the highest slope of the spike can occur during the ramp-up (Fig. 8(a)) as well as during the drop-off, after the maximum (Fig. 8(b)). The second recurrent shapes presents a plateau after a very steep ramp-up, that lasts 30–50 min and is characterized by many peaks of the same order of magnitude (Fig. 8(c)) or by secondary maxima after the main peak's occurrence (Fig. 8(d)). Fig. 8(e), (f) shows less frequent shapes, characterized by relatively slow increasing/decreasing ramps. Differently from the 10-min records, these events can also be subdivided according to the occurrence or not of a transition between different wind regimes during the 1-h period. Fig. 8(a), (c), (e) shows some examples of the non-transition case, in which the large short-lasting events are superimposed to a steady lower background flow. Fig. 8(b), (d), (f) shows some examples of transition cases between higher-to-lower (Fig. 8(b), (f)) or between lower-to-higher (Fig. 8(d)) wind speed regimes. Such transitions can be due, for instance, to mesoscale meteorological structures like fronts, which represent the passage between two different air masses and are usually associated with an intense convective activity sometimes organized in multi-cell systems, e.g. squall lines.

Studies are in progress to inspect the meteorological phenomena that can be associated to different thunderstorm shapes as well as to evaluate the response of structures to 10-min and 1-h thunderstorm records in order to clarify the actual role of the gust front time passage.

Table 5
Mean value and cov of the turbulence intensity.

Port	Anem. No.	$\langle \bar{I}_v \rangle$	Cov($\bar{I}_v$)
Genoa	1	0.10	0.40
	2	0.12	0.36
Livorno	1	0.10	0.35
	2	0.15	0.21
	3	0.08	0.21
	4	0.08	0.28
	5	0.13	0.26
Savona	1	0.14	0.22
	2	0.14	0.17
	3	0.14	0.64
	4	0.14	0.40
	5	0.13	0.66
La Spezia	2	0.18	0.20
	3	0.13	0.23
All ports		0.12	0.39

6. Turbulence intensity

The literature on thunderstorm outflows generally assigns $I_v = \bar{I}_v$, i.e. $\mu = 1$ (Eq. (6)) [17,38,40,41]. This is due to the weak dependence of I_v on the time, or better on its slowly-varying character, and to the persistent lack of suitable data. In this frame two problems mainly attracted research: the values assumed by $\bar{I}_v$ in the course of thunderstorm outflows as compared with those related to synoptic events and the dependence of this parameter on the height h AGL and on the roughness length z_0 [19,38,43–48].

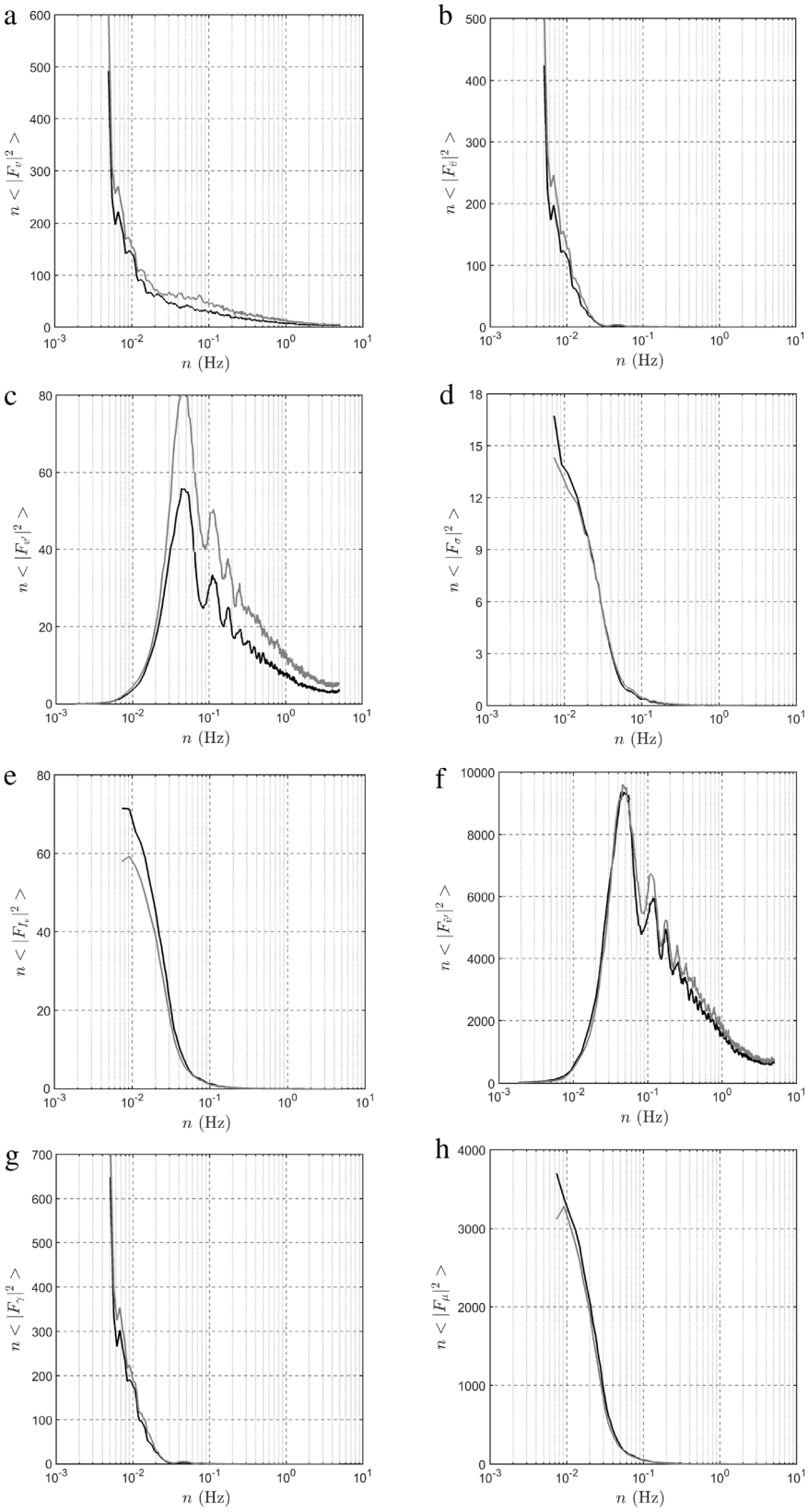

Fig. 5. Fourier analysis of decomposed thunderstorm signals: (a) v; (b) $\bar{v}$; (c) v'; (d) σ_v; (e) I_v; (f) $\tilde{v}'$; (g) γ; (h) μ.

Table 5 shows the mean value and the cov of the average turbulence intensity of the enlarged set of thunderstorm outflows gathered in this paper. The ensemble values in the last row of Table 5 confirm the previous average estimates, $\left\langle \bar{I}_v \right\rangle = 0.12$ [26], whereas they point out a larger spread, $\mathrm{cov}\left(\bar{I}_v\right) = 0.39$ vs. $\mathrm{cov}\left(\bar{I}_v\right) = 0.25$ [26], mostly depending on two new anemometers in the Port of Savona. This fact is not related to examining together 10-min and 1-h thunderstorms: their separation does not lead to any relevant difference in the results.

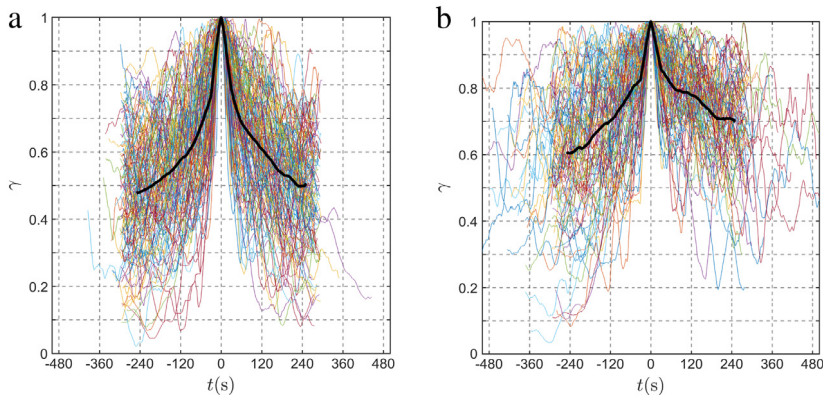

Fig. 6. Ensemble of the diagrams of γ for all the 10-min (a) and 1-h (b) thunderstorm records investigated, and their mean value (thick line).

However, a better comparison with the data obtained by analyzing synoptic events points out a key remark. If this analysis is carried out in the classic way, namely determining the residual fluctuation as the difference between the instantaneous velocity and the 10-min average, the new analysis fully confirms the previous results according to which the turbulence intensity of synoptic events is much greater than that of thunderstorm outflows. If, instead, likewise in the case of thunderstorm outflows, the residual fluctuation is extracted by a moving average period T = 30 s, the average turbulence intensity of synoptic events strongly decreases, $\left\langle \bar{I}_v \right\rangle = 0.11 - 0.13$, and closely approaches that of thunderstorm outflows. Studies on this matter are still in progress.

As far as concerns the dependence of the average turbulence intensity of thunderstorm outflows on the height AGL and on the roughness length, the results of the analyses are shown in Fig. 9(a). This picture collects the average values of the turbulence intensity of the thunderstorm outflows as a function of h/z_0, where the z_0 values are evaluated as described in [26], namely referring to neutral synoptic wind profiles and taking into account the local topography and upwind roughness features using the classic tools for synoptic winds [49–52]. Also in this case there is no relevant difference between 10-min and 1-h thunderstorms. The solid line in Fig. 9(a) refers to the classic expression of the turbulence intensity, $I_v = 1/\ln\left(h/z_0\right)$, as provided by many codes [53] for synoptic events and neutral atmospheric conditions. It is worth noticing that $\bar{I}_v$ exhibits a very weak trend according to which it seems to decrease on increasing h/z_0; this aspect was totally absent in Fig. 13(a) of [26]. Fig. 9(b) collects the average values of the turbulence intensity of the thunderstorm outflows as a function of the maximum value of the slowly-varying mean wind velocity, showing the absence of any relevant correlation between these quantities.

Fig. 10(a) shows the ensemble of the diagrams of μ for all the thunderstorm records investigated; also in this case no relevant difference occurs between the 10-min and 1-h thunderstorms. Fig. 10(b) provides the cov of μ as a function of t. Both the mean value and the cov of μ are nearly independent of time; this means that each diagram of μ can be regarded as a sample function of a stationary process. On the other hand, μ samples are not symmetric with respect to the mean, so their ensemble constitute a non-Gaussian process. Fig. 11 confirms this remark showing the detachment of the probability density function (pdf) of all the μ values from the reference Gaussian model. Table 6 enhances this aspect pointing out the detachment of the skewness and kurtosis of all the μ values from 0 and 3, respectively. This remark makes quite questionable the usual position $\mu = \bar{\mu} = 1$ adopted in literature. This topic is further briefly discussed in Section 8.

7. Reduced turbulent fluctuations

The statistical features of the reduced turbulent fluctuations $\tilde{v}'$ confirm that they reasonably constitute a stationary Gaussian random process with zero mean and unit standard deviation, as widely shared in literature [26], without pointing out any relevant difference between 10-min and 1-h thunderstorms.

Table 6
Mean value, standard deviation, skewness and kurtosis of all μ values.

Parameter	μ	σ_μ	γ_μ	κ_μ
Mean	1.000	0.293	0.568	2.872
Std	0.000	0.114	0.572	1.166

Table 7
Mean and std values of $\mu_{\tilde{v}'}$, $\sigma_{\tilde{v}'}$, $\gamma_{\tilde{v}'}$ and $\kappa_{\tilde{v}'}$ for the thunderstorm records.

Parameter	$\mu_{\tilde{v}'}$	$\sigma_{\tilde{v}'}$	$\gamma_{\tilde{v}'}$	$\kappa_{\tilde{v}'}$
Mean	−0.006	1.005	−0.100	2.841
Std	0.019	0.011	0.163	0.294

Fig. 12 shows the wavelet map (upper panel), multiplied by the frequency n, of the reduced turbulent fluctuations extracted from the 10-min (a) and 1-h (b) records (lower panel) detected by the anemometer 1 of the Port of Livorno during the downburst that occurred on 1 October 2012 [35]. Both signals are centered around the peak wind speed; the time–frequency representation is obtained through a wavelet transform generated by a Morlet-type analytic base; it denotes a stationary behavior and no significant change of the harmonic content along the time.

Table 7 shows, for all the thunderstorm records detected, the mean value and the standard deviation (std) of the mean value, std, skewness and kurtosis of $\tilde{v}'$ for $T = 30$ s. Accordingly, Fig. 13 points out the good agreement between the pdf of $\tilde{v}'$ and the reference Gaussian pdf.

The power spectral density (PSD) and the integral length scale of the reduced turbulent fluctuations $\tilde{v}'$ are determined on a sub-set of 128 10-min thunderstorm outflow records including an extremely low number of missing values; in the very few points in which the time series is interrupted, its continuity is obtained though linear interpolation.

The analysis of the harmonic content of $\tilde{v}'$ points out several aspects not adequately highlighted in [26]. In that study the PSD of $\tilde{v}'$ was given as a function of the reduced frequency $f = nz/\bar{v}_{\max}$, where z is the height of the anemometer and $\bar{v}_{\max}$ is the maximum value of the slowly-varying mean wind velocity. In addition, the integral scale of $\tilde{v}'$ was derived through a best fitting of the PSD and the model proposed in [21] for synoptic winds. It was found that the PSD of $\tilde{v}'$ extracted from thunderstorm outflow records perfectly follows the trend of the curve $n^{-5/3}$ in the inertial sub-range [17,19,38,40] whereas it does not capture the low frequency peak. It was also shown that the integral length scale of $\tilde{v}'$ extracted from thunderstorm outflow records, on average $L_v = 34.6$ m [26], is much less than the corresponding value evaluated for synoptic winds.

A more accurate study, carried out here on a richer and more controlled dataset, shows firstly that the parameterization of the PSD of $\tilde{v}'$ by the reduced frequency $f = nz/\bar{v}_{\max}$ (Fig. 14(a), (b)) is not the best choice. Better results can be obtained by expressing $S_{\tilde{v}'}$ as a function

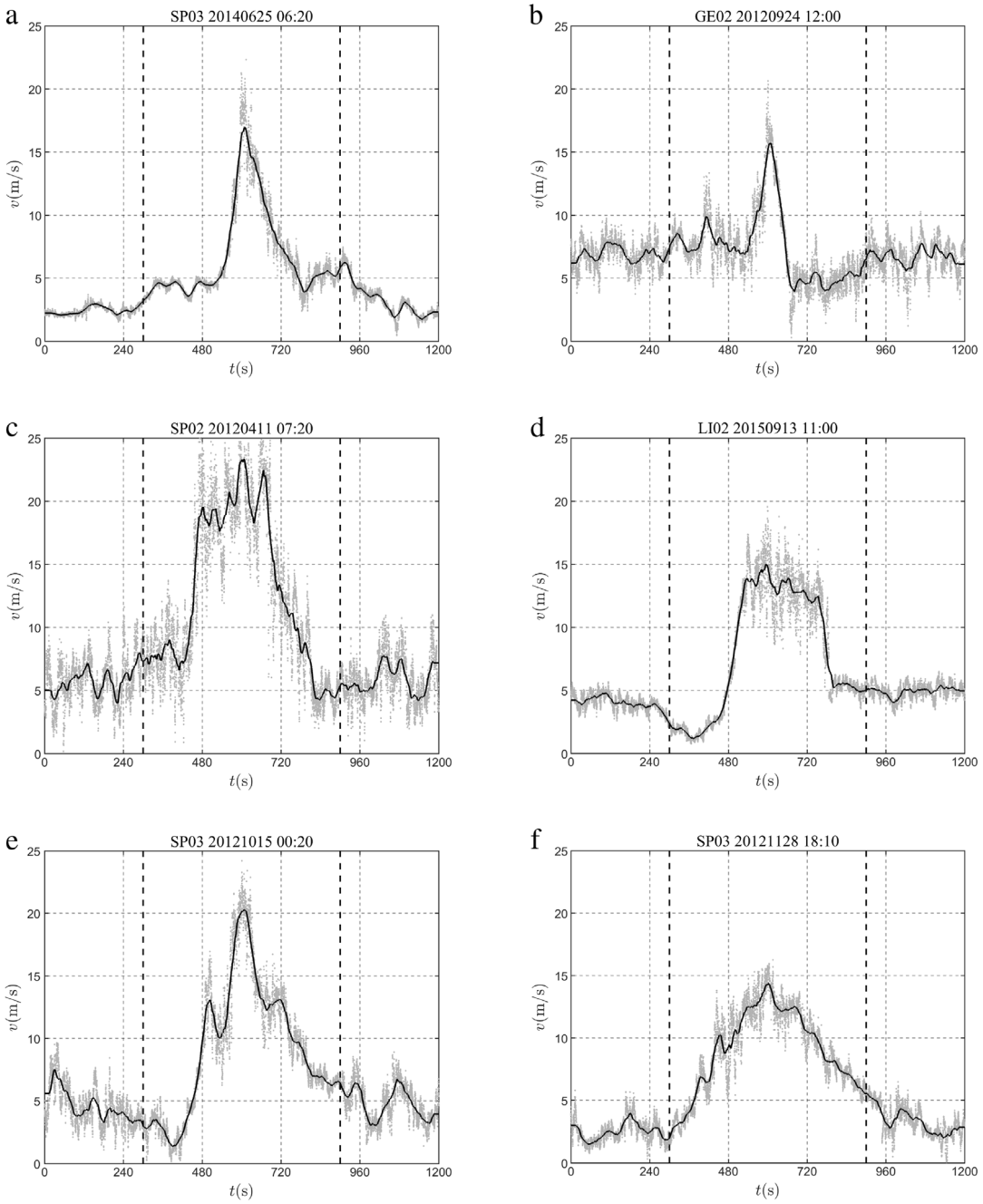

Fig. 7. Examples of 10-min thunderstorm records that present wind gusts with different shapes (the gray points denote the 20 min wind speed history; the black lines show the moving average wind speed; the vertical dashed lines include the 10-min time window around the peak).

of the reduced frequency $f = nL_v/\bar{v}_{\max}$ (Fig. 14(c), (d)), determining L_v from the auto-correlation function of $\tilde{v}'$. In fact, while Fig. 14(b) points out different peak positions for different sensors, Fig. 14(d) exhibits one dominant peak for all of them. Of course this approach is suitable provided that velocity records are available, whereas it becomes much more delicate when L_v should be evaluated by models, this quantity being very uncertain [21,54].

Table 8 compares the mean value and the cov of the integral length scale of $\tilde{v}'$ as detected by each anemometer and the whole network. Firstly, the time scale T_v of $\tilde{v}'$ is evaluated by integrating its normalized auto-correlation function from 0 until the time lag for which its value drops to 0.05 [55]; the integral length scale is then determined by invoking the Taylor's hypothesis, i.e. $L_v = \bar{v}_{\max} T_v$. Secondly, L_v is derived by the PSD fitting described above. In terms of mean values the integral length scale evaluated by the first method is even lower than that provided by the second one and in [26]. Instead, the standard deviation obtained through the first method is definitely less than that due to the first; this testifies a better stability and less uncertainties.

Likewise for the average turbulence intensity, a better comparison of these results with the data related to synoptic events points out a relevant remark. If the analysis is carried out by determining the residual fluctuation as the difference between the instantaneous velocity and the 10-min average, the new result confirms that the integral length scale of synoptic winds is much greater than that of thunderstorm outflows. If, instead, the residual fluctuation is extracted by a moving average period $T = 30$ s, the average integral length scale of synoptic winds strongly decreases, $\left\langle \bar{L}_v \right\rangle = 35$–$43$ m, and closely approaches that of thunderstorm outflows.

Fig. 15 shows two different representations of L_v as a function of h/z_0 (a) and $\bar{v}_{\max}$ (b). While no clear correlation is exhibited by

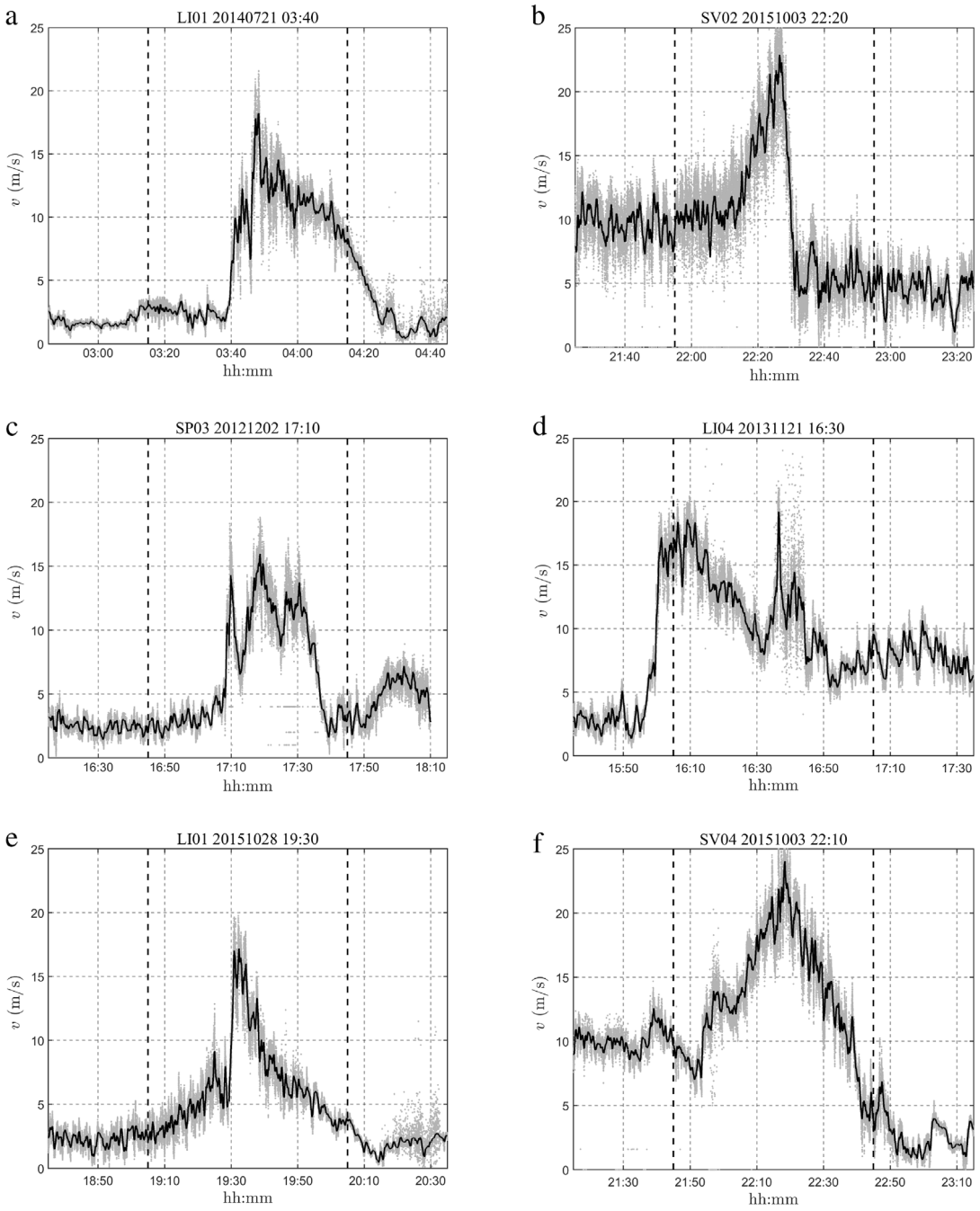

Fig. 8. Examples of 1-h thunderstorm records that present wind gusts with different shapes (the gray points denote the 2 h wind speed history; the black lines show the moving average wind speed; the vertical dashed lines include the 1-h time window around the peak).

Fig. 15(a), (b) shows that evaluating L_v through its auto-correlation this quantity increases on increasing $\bar{v}_{\max}$. This result matches the results provided by ESDU [49] for classic synoptic events and neutral atmospheric conditions.

8. Turbulence intensity modulation

Though $\tilde{v}'$ is well represented by a Gaussian (rapidly-varying) random process, according to Eq. (7) it is modulated by the non-Gaussian (slowly-varying) random process μ. Thus, $\mu\tilde{v}'$ is a non-Gaussian random process. Table 9 shows the mean value and the std of the mean, std, skewness and kurtosis of $\mu\tilde{v}'$ (for $T = 30$ s). Accordingly, Fig. 16 points out the detachment between the pdf of $\mu\tilde{v}'$ and its reference Gaussian pdf. Fig. 17 proves that the PSD of $\mu\tilde{v}'$ is very close to that of $\tilde{v}'$. Studies are in progress to clarify the role of this modulation on the wind loading and response of structures.

9. Noteworthy wind velocity ratios

Three wind velocity ratios were introduced in [26] that play a key role in the thunderstorm loading and response of structures [27–29]. They are defined by the relationships:

$$R = \frac{v_{\max}}{\hat{v}} \tag{8}$$

$$G_{\max} = \frac{v_{\max}}{\bar{v}_{\max}} \tag{9}$$

$$\hat{G}_v = \frac{\hat{v}}{\bar{v}_{\max}} \tag{10}$$

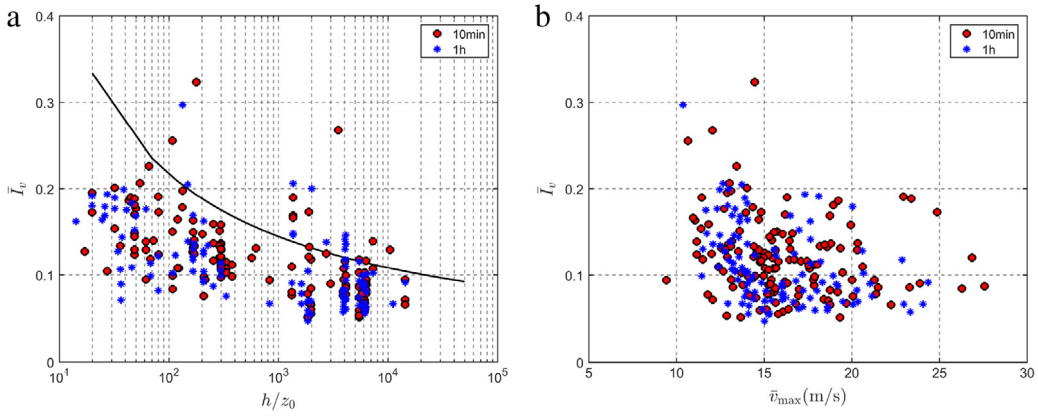

Fig. 9. Average turbulence intensity as a function of h/z_0 (a) and $\bar{v}_{\max}$ (b).

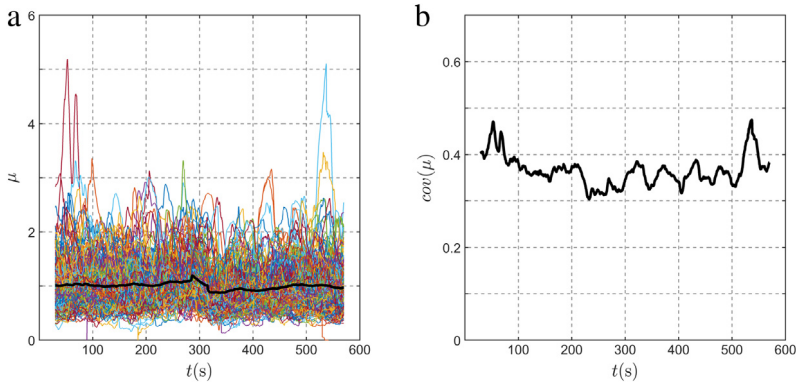

Fig. 10. (a) Ensemble of the diagrams of μ for all the thunderstorm records investigated and their mean value (thick line); (b) coefficient of variation of μ.

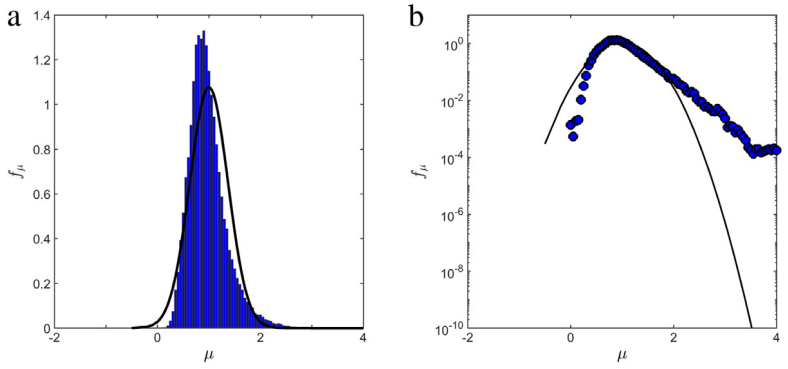

Fig. 11. Probability density function of μ for all the thunderstorm outflow records investigated: (a) decimal ordinate; (b) logarithmic ordinate.

where $v_{\max}$, $\hat{v}$ and $\bar{v}_{\max}$ are, respectively, the maximum sampled value of the wind velocity, the 1-s peak wind velocity and the maximum value of the slowly-varying mean wind velocity averaged on $T = 30$ s as shown in Fig. 18; $\hat{G}_v$ corresponds to the traditional definition of the gust factor for thunderstorm outflows [12,13,17,19]; $G_{\max} = R\hat{G}_v$.

Figs. 19 and 20 show two different representations of these three parameters as a function of h/z_0 and $\bar{v}_{\max}$, respectively. Fig. 19 confirms the result obtained in [26] exhibiting no clear correlation between the three wind velocity ratios and h/z_0. Fig. 20, instead, shows a moderate dependence according to which $G_{\max}$ and $\hat{G}_v$ tend to decrease on increasing $\bar{v}_{\max}$; this trend does not seem to involve the ratio R. Table 10 summarizes the mean value and the cov of R, $G_{\max}$ and $\hat{G}$. The values obtained herein perfectly match and confirm the previous ones [26].

10. Conclusions and prospects

Based upon the data detected by the monitoring network of the European Projects "Wind and Ports" and "Wind, Ports and Sea", this paper describes the extraction of 277 thunderstorm outflow records measured in the High Tyrrhenian Sea area by 14 ultra-sonic anemometers in the period 2011–2016. In this framework it repeats, improves and extends a previous preliminary study described in [26]. In particular, the present analysis is carried out by inspecting 10-min, 1-h and 10-h records centered around the peak wind speed; this approach pursues not only the creation of a more refined and controlled thunderstorm dataset but, even more, a major advance in the understanding of the thunderstorm time-scale and duration.

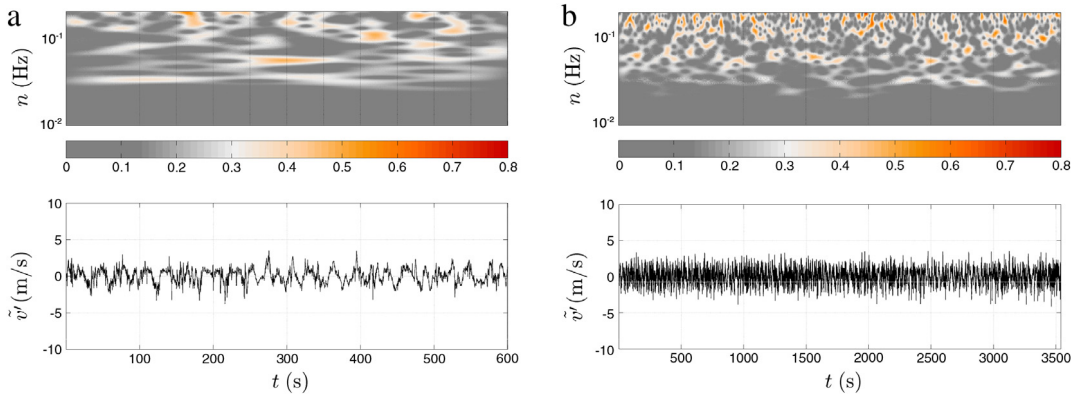

Fig. 12. Wavelet maps (upper panel) of the reduced turbulent fluctuation extracted from the 10-min (a) and 1-h (b) records (lower panel) detected by anemometer 1 of the Port of Livorno during the downburst occurred on October 1, 2012.

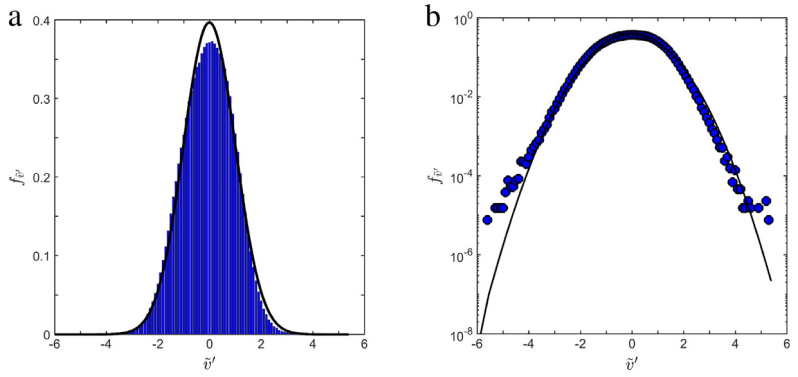

Fig. 13. Probability density function of $\tilde{v}'$ for all the thunderstorm outflow records detected: (a) decimal ordinate; (b) logarithmic ordinate.

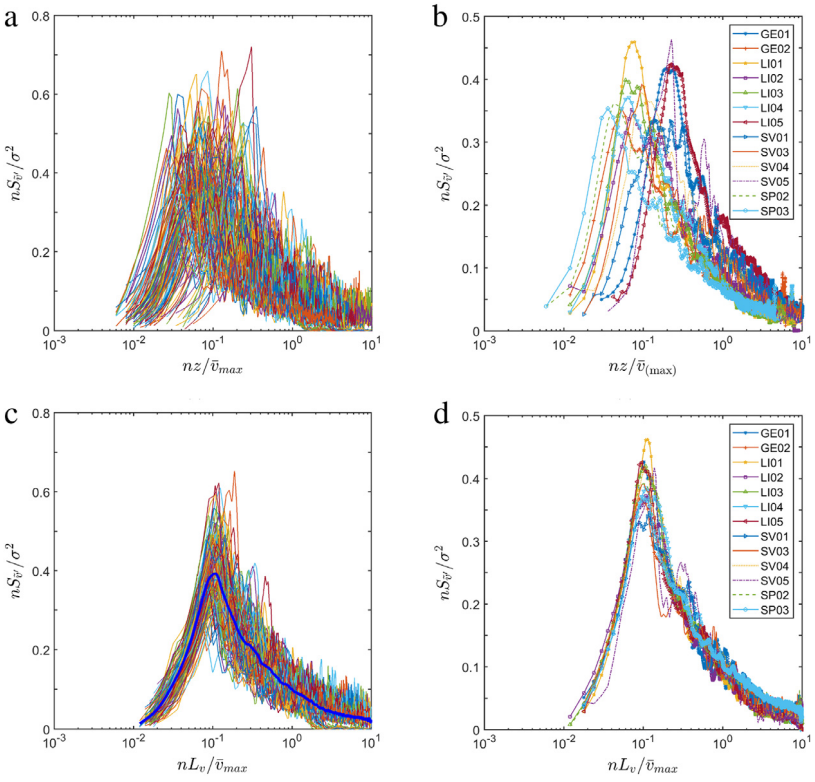

Fig. 14. PSD of $\tilde{v}'$ for different records and their mean value for every anemometer (b,d) and for all anemometers (c), as a function of $f = nz/\bar{v}_{\max}$ (a, b) and $f = nL_v/\bar{v}_{\max}$ (c, d).

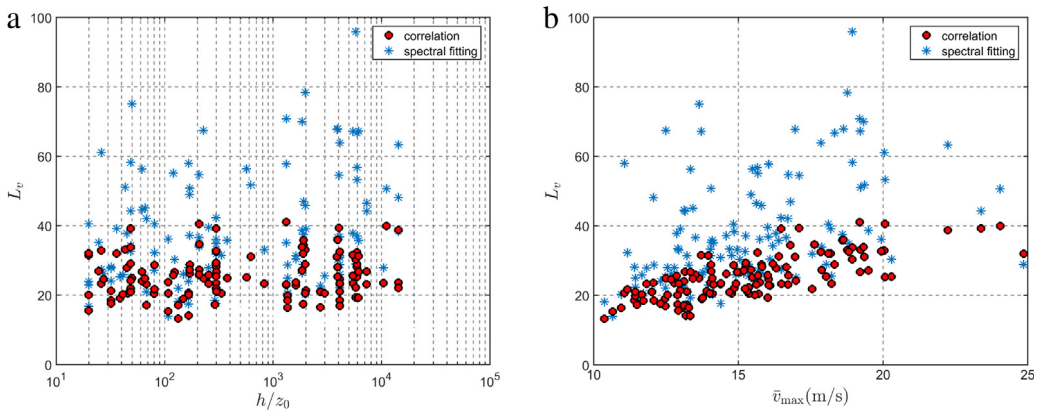

Fig. 15. Integral length scale as a function of h/z_0 (a) and $\bar{v}_{\max}$ (b).

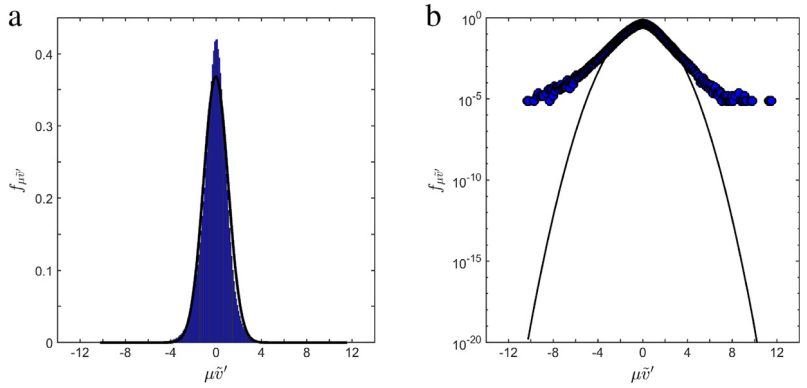

Fig. 16. Probability density function of $\mu\tilde{v}'$ for all the thunderstorm outflow records detected: (a) decimal ordinate; (b) logarithmic ordinate.

Table 8
Mean value and cov of the integral length scale of the reduced turbulent fluctuation.

Port	Anemometer No.	Autocorrelation		Spectral fitting	
		Mean(L_v) (m)	Cov(L_v)	Mean(L_v) (m)	Cov(L_v)
Genoa	1	30.27	0.24	42.87	0.24
	2	25.79	0.18	29.51	0.30
Livorno	1	29.70	0.13	46.44	0.36
	2	26.03	0.22	33.34	0.42
	3	29.76	0.19	48.21	0.45
	4	31.16	0.18	43.36	0.44
	5	31.73	0.20	52.70	0.43
Savona	1	29.30	0.31	31.00	0.18
	2	–	–	–	–
	3	28.19	0.17	36.20	0.34
	4	30.25	0.21	42.54	0.23
	5	25.75	0.07	37.94	0.22
La Spezia	2	27.11	0.27	30.26	0.40
	3	26.83	0.21	28.04	0.24
All ports		28.53	0.21	37.04	0.43

Table 9
Mean and std values of $\mu\tilde{v}'$, $\sigma_{\mu\tilde{v}'}$, $\gamma_{\mu\tilde{v}'}$ and $\kappa_{\mu\tilde{v}'}$ for the thunderstorm outflow records detected.

Parameter	$\mu\tilde{v}'$	$\sigma_{\mu\tilde{v}'}$	$\gamma_{\mu\tilde{v}'}$	$\kappa_{\mu\tilde{v}'}$
Mean	−0.025	1.063	−0.085	3.970
Std	0.035	0.046	0.414	1.480

In this regard thunderstorm outflow records are separated into 3 families depending on whether the presence of an evident peak associated with the gust front passage is clear in 10-min, 1-h or 10-h periods. This choice is relevant to investigate the slowly-varying mean wind velocity component whereas it is less important for the slowly-varying turbulence intensity and the rapidly-varying reduced turbulent fluctuation. In addition, thunderstorm outflows are separated into 4 groups depending on their peak wind speed. Results show no clear correlation between the duration of the most intense part of the record and the peak wind speed. It is worth noting, however, that the four events whose peak wind speed exceeds 30 m/s have a short duration. Signal analysis is restricted to the 10-min and 1-h thunderstorm outflows most relevant for the wind loading and response of structures.

The slowly-varying mean wind velocity records have been normalized by means of their maximum values. Despite their essential feature is a speed-up and -down of the wind speed, they exhibit an

Table 10
Mean values and covs of three wind velocity ratios for thunderstorms.

Port	Anemometer No.	Mean(R)	Cov(R)	Mean(G_{max})	Cov(G_{max})	Mean($\hat{G}$)	Cov($\hat{G}$)
Genoa	1	1.06	0.03	1.25	0.08	1.18	0.08
	2	1.06	0.03	1.29	0.10	1.22	0.08
Livorno	1	1.03	0.02	1.19	0.08	1.15	0.07
	2	1.07	0.04	1.31	0.10	1.22	0.08
	3	1.05	0.03	1.20	0.07	1.14	0.06
	4	1.03	0.02	1.17	0.06	1.13	0.05
	5	1.05	0.03	1.24	0.08	1.19	0.08
Savona	1	1.07	0.01	1.34	0.07	1.25	0.08
	2	1.03	0.03	1.39	0.10	1.35	0.10
	3	1.03	0.01	1.26	0.07	1.22	0.06
	4	1.04	0.02	1.28	0.07	1.23	0.07
	5	1.04	0.03	1.42	0.14	1.36	0.16
La Spezia	2	1.09	0.03	1.43	0.10	1.31	0.09
	3	1.08	0.04	1.35	0.10	1.26	0.08
All ports		1.05	0.04	1.27	0.11	1.21	0.09

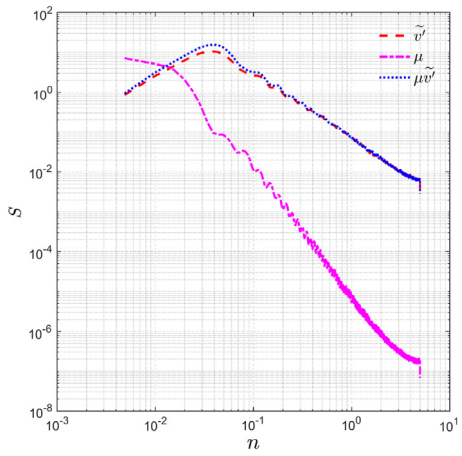

Fig. 17. PSD of μ, $\tilde{v}'$, $\mu\tilde{v}'$ for all the thunderstorm outflow records detected.

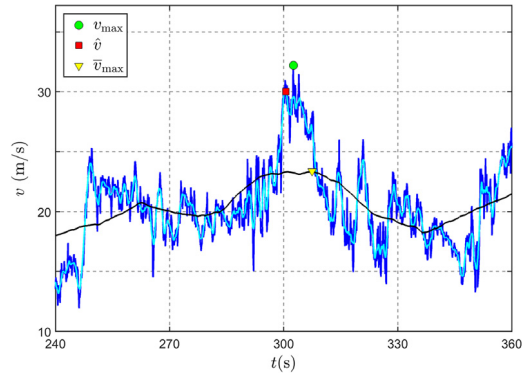

Fig. 18. Typical diagram of the wind velocity of thunderstorms: maximum value, v_{max}, 1-s peak, $\hat{v}$, and maximum value of the mean wind velocity averaged over $T = 30$ s, $\bar{v}_{max}$.

impressive spread. However, their mean values related to 10-min and 1-h thunderstorms are very similar in proximity of the peak whereas their difference is apparent far from it. These functions are crucial for defining quantitative criteria aiming to express the duration of the gust front passage likewise qualitative models to classify the different shapes of the thunderstorm outflow signature.

The study of the average turbulence intensity confirms the previous estimates though pointing out a larger spread. Differently from classic synoptic events, this quantity is nearly independent of the ratio between the height above ground level and the roughness length. Instead it is shown that higher values related to synoptic winds are fictitious. Dealing with them likewise for thunderstorm records, namely extracting the fluctuations by a moving average period, their average turbulence intensity decreases and closely approaches that of the thunderstorm outflows. As far as concerns the ratio between the slowly varying turbulence intensity and its mean value, the set of these signals can be regarded as a random stationary non-Gaussian process. This remark makes quite questionable the usual hypothesis adopted in literature according to which the turbulence intensity is identified with its average value.

Based upon a sub-set of 128 10-min thunderstorm outflow records including a very low number of missing values it is fully confirmed that the reduced turbulent fluctuation is a stationary Gaussian process and its PSD almost perfectly follows the trend of the curve $n^{-5/3}$ in the inertial sub-range. Differently from previous analyses, instead, it is shown that the parameterization of the PSD by the reduced frequency $f = nz/\bar{v}_{max}$ is not the best choice and better results are obtained by expressing this quantity as a function of the reduced frequency $f = nL_v/\bar{v}_{max}$, where the integral length scale L_v is evaluated by means of the auto-correlation function of the reduced turbulent fluctuations.

Likewise the average turbulence intensity also the integral length scale of the reduced turbulent fluctuation is almost independent of the ratio between the height above ground and the roughness length of the terrain. Besides, higher values related to synoptic events are fictitious as well. Dealing with them by extracting the turbulent fluctuations through a moving average period, their integral length scale decreases and closely approaches that of thunderstorm outflows.

Finally, also the three wind velocity ratios considered here for estimating the wind loading and response of structures, these including the gust factor, do not exhibit any relevant dependence on the ratio between the height above ground and the roughness length of the terrain.

It is worth noting, instead, a remark not pointed out by previous analyses. Whereas the average turbulence intensity does not exhibit any relevant dependence on the mean wind velocity, the integral length scale and the gust factors tend to increase on increasing this quantity.

Overall, the creation of an extended and more controlled dataset of thunderstorm outflow records provides robust and reliable estimates of the statistical properties of their signals and components parts. This represents a fundamental step forward towards the implementation of statistical models of thunderstorm downbursts adhering to the reality of these complex phenomena. It should be noted, however, that using single wind velocity records provides excellent insights into their time-histories but no element concerning their space dependence. The extension of such models to the time–space structure of the wind field calls for field acquisitions based on anemometer antennas and LiDAR profilers, likewise for downburst simulations carried out in wind tunnel facilities and by CFD.

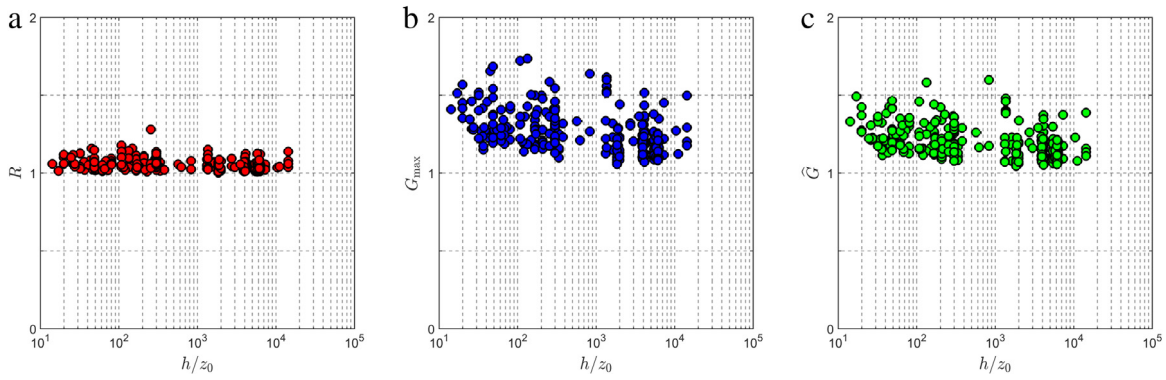

Fig. 19. Wind velocity ratios for thunderstorm outflows as functions of h/z_0: (a) R; (b) $G_{\max}$; (c) $\hat{G}$.

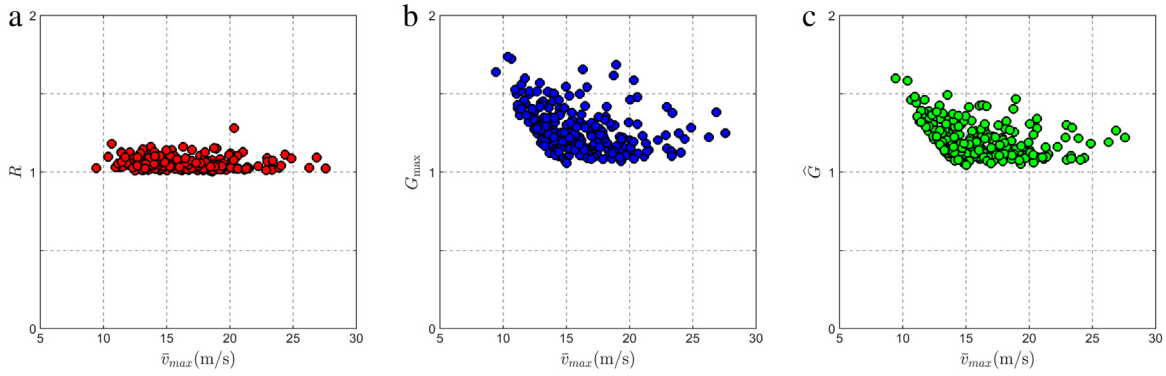

Fig. 20. Wind velocity ratios for thunderstorm outflows as functions of $\bar{v}_{max}$: (a) R; (b) $G_{\max}$; (c) $\hat{G}$.

Acknowledgments

This research has been carried out in the framework of the Project "Wind monitoring, simulation and forecasting for the smart management and safety of port, urban and territorial systems" (Grant Number 2015.0333, ID ROL: 9820), funded by Compagnia di San Paolo, of the Project "Identification and diagnostic of complex structural systems" (Grant Number 2015TTJN95), funded by the Italian Ministry of Instruction and Scientific Research (PRIN 2015) and of the 111 Project, funded by the Ministry of Education, China, under the leadership of Prof. Qingshan Yang. The anemometric data have been recorded through the wind monitoring network of the European Projects "Wind and Ports" and "Wind, Ports, and Sea", funded by the Cross-border Cooperation Program "Italy-France Maritime 2007–2013".

References

[1] C.W. Letchford, C. Mans, M.T. Chay, Thunderstorms–their importance in wind engineering (a case for the next generation wind tunnel), J Wind Eng Ind Aerodyn 90 (2002) 1415–1433.
[2] G. Solari, Emerging issues and new scenarios for wind loading on structures in mixed climates, Wind Struct 19 (2014) 295–320.
[3] A.G. Davenport, The application of statistical concepts to the wind loading of structures, Proc Inst Civ Eng 19 (1961) 449–472.
[4] T.T. Fujita, Downburst: Microburst and macroburst, University of Chicago Press, Chicago, IL, 1985.
[5] T.T. Fujita, Downburst: meteorological features and wind field characteristics, J Wind Eng Ind Aerodyn 36 (1990) 75–86.
[6] R.G. Goff, Vertical structure of thunderstorm outflows, Mon Weather Rev 104 (1976) 1429–1440.
[7] H.C.S. Thom, New distributions of extreme wind speeds in the United States, J Struct Div 94 (1968) 1787–1801 ASCE.
[8] L. Gomes, B.J. Vickery, On thunderstorm wind gusts in Australia, Civ Eng Trans Ind Eng Aust 18 (1976) 33–39.
[9] L.A. Twisdale, P.J. Vickery, Research on thunderstorm wind design parameters, J Wind Eng Ind Aerodyn 41 (1992) 545–556.
[10] E.C.C. Choi, Extreme wind characteristics over Singapore - an area in the equatorial belt, J Wind Eng Ind Aerodyn 83 (1999) 61–69.
[11] F.T. Lombardo, J.A. Main, E. Simiu, Automated extraction and classification of thunderstorm and non-thunderstorm wind data for extreme-value analysis, J Wind Eng Ind Aerodyn 97 (2009) 120–131.
[12] E.C.C. Choi, Wind characteristics of tropical thunderstorms, J Wind Eng Ind Aerodyn 84 (2000) 215–226.
[13] E.C.C. Choi, F.A. Hidayat, Gust factors for thunderstorm and non-thunderstorm winds, J Wind Eng Ind Aerodyn 90 (2002) 1683–1696.
[14] E.C.C. Choi, Field measurement and experimental study of wind speed during thunderstorms, J Wind Eng Ind Aerodyn 92 (2004) 275–290.
[15] V. Duranona, M. Sterling, C.J. Baker, An analysis of extreme non-synoptic winds, J Wind Eng Ind Aerodyn 95 (2006) 1007–1027.
[16] K.D. Orwig, J.L. Schroeder, Near-surface wind characteristics of extreme thunderstorm outflows, J Wind Eng Ind Aerodyn 95 (2007) 565–584.
[17] J.D. Holmes, H.M. Hangan, J.L. Schroeder, C.W. Letchford, K.D. Orwig, A forensic study of the Lubbock-Reese downdraft of 2002, Wind Struct 11 (2008) 19–39.
[18] L. Jarvi, A.J. Punkka, D.M. Schultz, T. Petaja, H. Hohti, J. Rinne, T. Pohja, M. Kulmala, P. Hari, T. Vesala, Micrometeorological observations of a microburst in southern Finland, Bound Layer Meteorol 125 (2007) 343–359.
[19] F.T. Lombardo, D.A. Smith, J.L. Schroeder, K.C. Mehta, Thunderstorm characteristics of importance to wind engineering, J Wind Eng Ind Aerodyn 125 (2014) 121–132.
[20] W.S. Gunter, J.L. Schroeder, High-resolution full-scale measurements of thunderstorm outflow winds, J Wind Eng Ind Aerodyn 138 (2015) 13–26.
[21] G. Solari, G. Piccardo, Probabilistic 3-D turbulence modeling for gust buffeting of structures, Probab Eng Mech 16 (2001) 73–86.
[22] G. Solari, F. Tubino, A turbulence model based on principal components, Probab Eng Mech 17 (2002) 327–335.
[23] G. Solari, M.P. Repetto, M. Burlando, P. De Gaetano, M. Pizzo, M. Tizzi, M. Parodi, The wind forecast for safety management of port areas, J Wind Eng Ind Aerodyn 104–106 (2012) 266–277.
[24] M.P. Repetto, M. Burlando, G. Solari, P. De Gaetano, M. Pizzo, M. Tizzi, A GIS-based platform for the risk assessment of structures and infrastructures exposed to wind, Adv Eng Softw (2017). http://dx.doi.org/10.1016/j.advengsoft.2017.03.002. (in press).
[25] P. De Gaetano, M.P. Repetto, T. Repetto, G. Solari, Separation and classification of extreme wind events from anemometric records, J Wind Eng Ind Aerodyn 126 (2014) 132–143.

[26] G. Solari, M. Burlando, P. De Gaetano, M.P. Repetto, Characteristics of thunderstorms relevant to the wind loading of structures, Wind Struct 20 (2014) 763–791.
[27] G. Solari, P. De Gaetano, M.P. Repetto, Thunderstorm response spectrum: fundamentals and case study, J Wind Eng Ind Aerodyn 143 (2015) 62–77.
[28] G. Solari, Thunderstorm response spectrum technique: theory and applications, Eng Struct 108 (2016) 28–46.
[29] G. Solari, D. Rainisio, P. De Gaetano, Hybrid simulation of thunderstorm outflows and wind-excited response of structures. Meccanica, 2017, http://dx.doi.org/10.1007/s11012-017-0718-x (in press).
[30] N.J. Cook, Review of errors in archived wind data, Weather 69 (2014) 72–78.
[31] N.J. Cook, Detecting artifacts in analyses of extreme wind speeds, Wind Struct 19 (2014) 271–294.
[32] M. Burlando, A. De Cio, M. Pizzo, G. Solari, Analysis of the wind vertical profile of thunderstorm events in the Mediterranean, In: Proc. 9th Asia-Pacific conf. on wind engineering, Auckland, 2017, (submitted for publication).
[33] L. Gomes, B.J. Vickery, Extreme wind speeds in mixed climates, J Ind Aerod 2 (1977/1978) 331–344.
[34] M. Kasperski, A new wind zone map of Germany, J Wind Eng Ind Aerodyn 90 (2002) 1271–1287.
[35] M. Burlando, D. Romanic, G. Solari, H. Hangan, S. Zhang, Field data analysis and weather scenario of a downburst event in Livorno, Italy on 1 October 2012, Mon Weather Rev (2017). http://dx.doi.org/10.1175/MWR-D-17-0018.1.
[36] J.D. Riera, L.F. Nanni, Pilot study of extreme wind velocities in a mixed climate considering wind orientation, J Wind Eng Ind Aerodyn 32 (1989) 11–20.
[37] V. Durañona, The significance of non-synoptic winds in the extreme wind climate of Uruguay, In: Proc. 14th int. conf. on wind engineering, Porto Alegre, Brasil, 2015.
[38] D.K. Kwon, A. Kareem, Gust-front factor: new framework for wind load effects on structures, J Struct Eng 135 (2009) 717–732 ASCE.
[39] E.C.C. Choi, F.A. Hidayat, Dynamic response of structures to thunderstorm winds, Prog Struct Eng Mater 4 (2002) 408–416.
[40] L. Chen, C.W. Letchford, A deterministic-stochastic hybrid model of downbursts and its impact on a cantilevered structure, Eng Struct 26 (2004) 619–629.
[41] L. Chen, C.W. Letchford, Numerical simulation of extreme winds from thunderstorm downbursts, J Wind Eng Ind Aerodyn 95 (2007) 977–990.
[42] M. Mccullough, D.K. Kwon, A. Kareem, L. Wang, Efficacy of averaging interval for non-stationary winds, J Wind Eng Ind Aerodyn 140 (2013) 1–19.
[43] M.T. Chay, F. Albermani, R. Wilson, Numerical and analytical simulation of downburst wind loads, Eng Struct 28 (2006) 240–254.
[44] G.S. Wood, K.C.S. Kwok, N.A. Motteram, D.F. Fletcher, Physical and numerical modelling of thunderstorm downbursts, J Wind Eng Ind Aerodyn 89 (2001) 535–552.
[45] J. Kim, H. Hangan, Numerical simulations of impinging jets with application to downbursts, J Wind Eng Ind Aerodyn 95 (2007) 279–298.
[46] Z. Xu, H. Hangan, Scale, boundary and inlet condition effects on impinging jets, J Wind Eng Ind Aerodyn 96 (2008) 2383–2402.
[47] M.S. Mason, G.S. Wood, D.F. Fletcher, Numerical simulation of downburst winds, J Wind Eng Ind Aerodyn 97 (2009) 523–539.
[48] B.C. Vermeire, L.G. Orf, E. Savory, Improved modelling of downburst outflows for wind engineering applications using a cooling source approach, J Wind Eng Ind Aerodyn 99 (2011) 801–814.
[49] Engineering Sciences Data Unitc, Computer program for wind speeds and turbulence properties: flat or hill sites in terrain with roughness changes, ESDU Item 92032, London UK, 1993.
[50] F. Castino, L. Rusca, G. Solari, Wind climate micro-zoning: A pilot application to Liguria Region (North-Western Italy), J Wind Eng Ind Aerodyn 91 (2003) 1353–1375.
[51] M. Burlando, L. Carassale, E. Georgieva, C.F. Ratto, G. Solari, A simple and efficient procedure for the numerical simulation of wind fields in complex terrain, Bound Layer Meteorol 125 (2007) 417–439.
[52] M. Burlando, P. De Gaetano, M. Pizzo, M.P. Repetto, G. Solari, M. Tizzi, Wind climate analysis in complex terrain, J Wind Eng Ind Aerodyn 123 (2013) 349–362.
[53] Eurocode 1, Actions on structures–General actions, Part 1-4: Wind actions, CEN, EN 1991–1-4, 2005.
[54] L.C. Pagnini, G. Solari, Gust buffeting and turbulence uncertainties, J Wind Eng Ind Aerodyn 90 (2002) 441–459.
[55] R.G.J. Flay, D.C. Stevenson, Integral length scales in strong winds below 20 m, J Wind Eng Ind Aerodyn 28 (1988) 21–30.